Micromagnetic study of spin-wave dispersion engineering and magnon confinement in YIG magnonic crystals

Author: Antoni Homar Genovart, ahomarge13@alumnes.ub.edu
Facultat de Física, Universitat de Barcelona, Diagonal 645, 08028 Barcelona, Spain.

Advisor: Marius V. Costache, costache@ub.edu

Abstract: This work investigates magnonic crystals based on nanostructured Yttrium Iron Garnet (YIG) waveguides through micromagnetic simulations performed with mumax3. Two main objectives are addressed: engineering controllable spin-wave band structures and spatially confining magnons in a cavity. The structures consist of a YIG waveguide patterned with a one-dimensional periodic array of holes of varying geometry. For rectangular holes, a lower flat band emerges whose frequency decreases with increasing hole width, providing a geometric tuning knob; this tunability is exploited to design a magnon cavity that confines magnons at a defect site via a quadratic taper. Concave and elliptical geometries yield quasi-gapless, thin-film-like dispersions, identified as the most suitable candidates for magnon Rayleigh–Jeans condensation, which preliminary parametric-pumping simulations did not yet achieve.

Keywords: Magnons, Spin waves, Magnonic crystals, Bose–Einstein condensation, Micromagnetic simulations, Condensed matter physics
SDGs: SDG 7: Affordable and Clean Energy, Target 7.3; SDG 9: Industry, Innovation and Infrastructure, Target 9.5.

I. INTRODUCTION

Magnons are collective excitations of an ordered spin lattice. They are quasiparticles: like particles, they are described by a dispersion relation and carry a well-defined quasi-momentum, but unlike elementary particles they require a material medium in which to be defined, created and propagated. Hence, magnons can only exist in magnetically ordered media. So magnonic crystals enable control over spin-wave dynamics by introducing periodic variations in the magnetic properties of the medium. Further characterization of magnons detailed in Sec. II.

This work pursues two main objectives. The first is to characterize how the spin-wave dispersion relation of a one-dimensional magnonic crystal depends on the geometry of the periodic patterning, specifically on the hole width and size, the lattice constant and the inter-hole spacing. The relevant features are the position of the bands, the emergence of flat bands and the opening of tunable band gaps. The aim is to obtain controllable, engineered band structures that serve as a basis for the subsequent study of magnon dynamics and, ultimately, magnon condensation (RJC) [1].
The second objective is to design a magnonic cavity by adiabatically tapering the hole geometry, so as to spatially confine magnons at a defect site. This confined mode is intended as a building block for future magnon–photon–phonon (optomagnomechanical) interactions.

The material used in this work is Single-crystal Yttrium Iron Garnet (YIG). YIG is a ferrimagnetic insulator with cubic-crystal symmetry that combines a uniquely low magnon damping with a high Curie temperature Tc=560K. Magnons are considered as relatively weakly interacting bosonic quasiparticles at temperatures far below Tc, so a high Tc is beneficial because they can thermalize through four-magnon scattering processes and form a Bose–Einstein condensate (BEC) when the number of magnons is high enough. At room temperature, where mode occupations are large, this transition is more accurately described as a Rayleigh–Jeans condensation (RJC), the regime considered in this work [1].

The control of magnons enabled by these structures underpins several applications. The most direct is microwave-to-optical quantum transduction, allowing superconducting quantum processors to interface with optical-fibre networks [2]. Other applications may be quantum memories (long magnon lifetimes in low-damping materials) [3], ultra-sensitive magnetometry and spectroscopy [4], axion dark-matter detection (axion–magnon coupling) [5] and finally magnonic computing with low energy dissipation as no charge transport is involved [6].

II. THEORETICAL BACKGROUND

To introduce magnons, consider a d-dimensional lattice described by the isotropic Heisenberg Hamiltonian with nearest-neighbour interactions [1]

$$\hat{\mathcal{H}} = -J \sum_{\langle i,j \rangle} \left[\hat{S}_i^x \hat{S}_j^x + \frac{1}{2} \left(\hat{S}_i^+ \hat{S}_j^- + \hat{S}_i^- \hat{S}_j^+ \right) \right] \tag{1}$$

where the quantization axis is taken along x (the saturation direction) and $\hat{S}^{\pm} \equiv \hat{S}^y \pm i\hat{S}^z$.

Solving it is beyond the scope of this work, but it simplifies to

$$\hat{\mathcal{H}} = E_0 + 2zJS\sum_{\vec{k}}[1-\gamma(\vec{k})]\hat{a}^\dagger_{\vec{k}}\hat{a}_{\vec{k}}, \quad \gamma(\vec{k}) = \frac{1}{z}\sum_j e^{i\vec{k}\cdot\vec{t}_j} \tag{2}$$

Where $E_0 = -zJNS^2$ is the ground-state energy, $\hat{a}^\dagger_{\vec{k}}$ and $\hat{a}_{\vec{k}}$ are the bosonic creations and annihilation operators, $\gamma(\vec{k})$ is a geometric factor that depends on the lattice and $\vec{t} = \vec{r_j} - \vec{r_i}$.
This Hamiltonian describes a set of independent harmonic oscillators with frequency

$$\hbar\omega(\vec{k}) = 2zJS[1-\gamma(\vec{k})] \tag{3}$$

And the quantum of energy $h\omega(\vec{k})$ is called magnon. Dipolar, spin-orbit (anisotropy) and Zeeman interactions are not included analytically but are fully accounted for in the micromagnetic simulations [1].

III. METHODS

To simulate the magnetic properties an open-source GPU-accelerated software MuMax 3.0 is used. It uses the Landau-Lifshitz-Gilbert (LLG) equation to model magnetization dynamics

$$\frac{\mathrm{d}\vec{m}}{\mathrm{d}t} = -\gamma\frac{1}{1+\alpha^2}\left\{\vec{m}\times\vec{B}_{\text{eff}} + \alpha\left[\vec{m}\times\left(\vec{m}\times\vec{B}_{\text{eff}}\right)\right]\right\} \tag{4}$$

where $\vec{m} = \vec{m}(\vec{r}, t)$ is the magnetization vector, γ is the gyromagnetic ratio and α is the Gilbert damping constant. $\vec{B}_{\text{eff}} = \vec{B}_{\text{ext}} + \vec{B}_{\text{exch}} + \vec{B}_{\text{demag}}$ is the effective field. Here $\vec{B}_{\text{ext}}$ is the applied (Zeeman) field, $\vec{B}_{\text{exch}} = \frac{2A_{ex}}{M_s}\nabla^2\vec{m}$ is the exchange field, and $\vec{B}_{\text{demag}}$ is the demagnetizing (dipolar) field generated by the magnetic charges that arise wherever the magnetization is non-uniform or meets a boundary. This last term plays a central role in this work: the patterned holes create localized magnetic charges whose demagnetizing field governs the formation of flat bands.

The materials parameters are exchange constant $A_{ext} = 3.4$ pJ/m, saturation magnetization $M_{sat} = 138$ kA/m, Gilbert damping $\alpha = 0.0005$ and temperature $T = 300$ K [Appendix E].
To extract the magnon dispersion relation for the different geometries, a short magnetic field pulse is applied along the y-axis, Gaussian in both space and time. It has an amplitude of $B_0 = 10$ mT and cutoff frequency of $f_c \approx 16$ GHz, ensuring excitation of all magnon modes within the range of interest ($f \leq 10$ GHz). The dispersion relation can be obtained by averaging the y-component of the magnetization vector along the y and z axis, and then performing the Fast Fourier Transform in time and space (x-axis). All the results are for an external magnetic field of $B_{ext} = 150$ mT.

IV. RESULTS

A. Rectangular holes

As a reference, the spin-wave dispersion of an in-plane magnetized thin film, with k along the magnetization, starts from the finite Kittel frequency at $k = 0$ [7], decreases with $|k|$ owing to the dipolar interaction down to a minimum at $k_{\min}$, and then rises as the exchange term ($\propto k^2$) dominates; it is symmetric in $\pm k$ [1] [Appendix A].
If a periodic array of holes is introduced, we expect the dispersion to develop flatter bands and band gaps, corresponding to the extended Bloch magnon modes of the crystal or resonant modes. To study how these band gaps and flat bands depend on the hole width along the x direction, we define a unit cell containing a rectangular hole at its centre [Fig. 1]. The simulated crystals consist of 50 unit cells, each of size $640 \times 640 \times 400$nm. The hole height is fixed at 260 nm while its width is varied between 100 and 500 nm [Appendix A]. The simulation grid consists of $2048 \times 64 \times 8$ cells resulting on $15.624 \times 10 \times 50$nm cell size. The lateral cell dimensions are kept below the exchange length of YIG, $l_{\text{ex}} \approx 18$ nm, ensuring a valid discretization of the exchange interaction. Along z, the cell size exceeds l_{ex}; this is justified because the modes of interest are uniform across the film thickness, so no exchange gradients need to be resolved in that direction.

The most prominent feature is the appearance of resonant mode leading to a lower flat band. The sharp vertical edges of the rectangular holes, perpendicular to the magnetization, host intense magnetic surface charges ($\vec{M}\cdot\hat{n} \neq 0$). The resulting local demagnetizing field opposes the applied field, lowering the internal field around each hole and creating a potential well that traps magnons locally, originating the flat bands and the edge-localized mode profiles observed in real space.
As the hole width increases the two charged faces move apart, their dipolar fields cancel less effectively and the demagnetizing field penetrates deeper into the material. This creates a deeper and wider well that lowers the frequency of the trapped magnons. As a consequence this flat band shifts towards lower frequencies.

We focus our attention on the lower flat band for two reasons. The first one is that these may be interesting modes for building a cavity: if its frequency can be tuned at will, one can design a defect such that the central region, where magnons are to be confined, has its lower flat band lying within a band gap of the surrounding

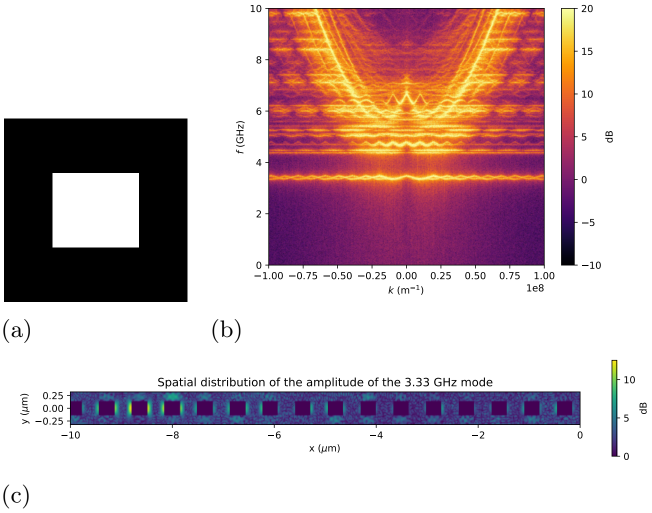

FIG. 1: (a) Unit cell of the rectangular geometry, with a 300×260 nm hole in a 640×640 nm cell. (b) Magnon dispersion relation of the crystal. The lower flat band appears at $\sim$3.33 GHz. (c) Spatial distribution of the 3.33 GHz mode amplitude, corresponding to the lower flat band.

geometry, which prevents magnon propagation and thus acts as a mirror. Moreover, a flat band implies a vanishing group velocity ($d\omega/dk \approx 0$, magnon trapped in a potential well); the corresponding magnons are essentially non-propagating which makes them perfect candidates for spatial confinement. Beyond cavity confinement, removing this band, in turn, is relevant for condensation, as discussed in Sec. IV.D.

Several further differences with respect to the thin film are observed. The thin film dispersion relation is still present, but its linewidth is significantly broader with interference-like structures related to the system's geometry. This broadening may have two origins. Along the frequency axis from periodic patterning modulation. Along the wave-vector axis spatial localization translates into delocalization in k. This dispersion is also shifted towards higher frequencies the wider the hole width is. Between the lower flat band and the minimum of the dispersion, additional flat bands appear, separated by band gaps. Finally, more of these additional flat bands appear as the hole width increases, since the lower flat band shifts down and the quadratic branch shifts up, broadening the frequency window between them.

1. *Magnon cavity*

Based on the previous results [Appendix A], we construct a cavity consisting of 9 mirror cells on each side (400 nm hole width), 2 central defect cells (200 nm hole width), and 10 transition cells on each side (total length 25.60 μm). The value of the x grid size N_x has been increased to 4096 for more resolution. The hole width of the transition cells follows a quadratic profile between the mirror and the central cells. This adiabatic taper minimizes the magnonic impedance mismatch between the mirror and defect cells, suppressing the reflections and scattering that an abrupt geometry change would cause and thereby maximizing the Q-factor of the cavity mode [Fig. 2].

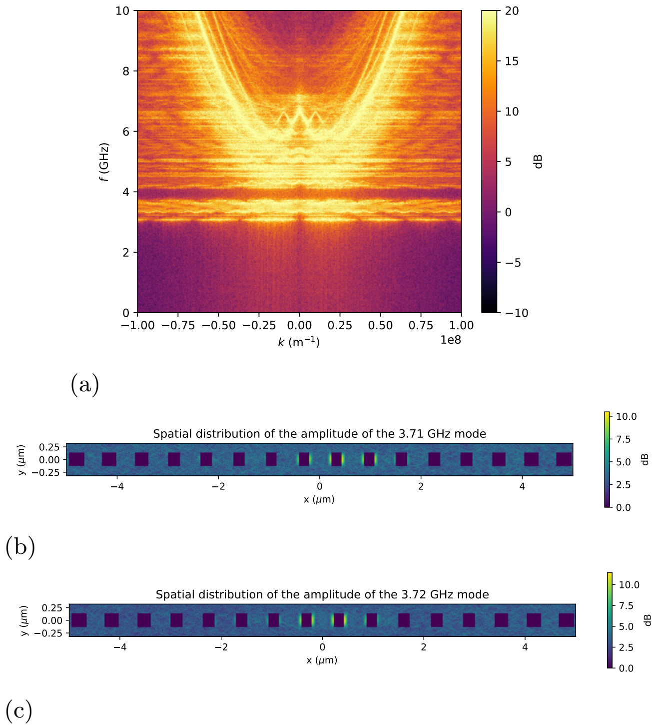

FIG. 2: (a) Magnon dispersion relation of the cavity structure. Spatial distribution of the confined mode at (b) 3.71 and (c) 3.72 GHz, localized at the central defect region. See other modes at Appendix D.

The dispersion relation shows a set of closely spaced flat bands between 3.10 and 3.75 GHz, each corresponding to the local lower flat band of a transition cell, whose frequency varies with the hole width along the taper. In the real-space representation we observe that the modes at frequencies 3.71 and 3.72 GHz (originating from the engineered lower flat band) are localized at the centre of the cavity. These modes lie within the band gap of the mirror cells and therefore cannot propagate into them, remaining confined to the defect region, where the mechanical modes of the magnomechanical design would also be localized [1]. The structure thus acts as a magnonic cavity, co-localizing magnons with the mechanical modes. By tuning the static external magnetic field, the frequency of these confined modes can be brought into resonance with the breathing mechanical mode ($\omega_m \approx \omega_b$), the regime in which the linear magnomechanical coupling is maximized. The coupling strength itself is not evaluated here and is left for future work; these results establish the spatial confinement and co-localization that are a prerequisite for it.

B. Concave holes

We now focus on removing this lower flat band, in order to obtain a dispersion relation as close as possible to that of the thin film while keeping a periodic array of holes.
From the previous geometry we observed that the narrower the central hole, the higher the frequency of the lower flat band, bringing it closer to the quadratic branch. However, even for the narrowest rectangle (100 nm) a sizeable band gap remains between the two.
We therefore propose a geometry based on the 300 nm rectangle, to which we add two semi-ovals of magnetic material on each side of the hole. The 300 nm rectangle is chosen in order to have enough central spacing to insert the semi-ovals. These allow the central spacing to be reduced further than the narrowest rectangle permits, pushing the lower flat band closer to the quadratic branch. To study the dependence of the lower flat band on this central spacing, the vertical semi-axis of the oval is kept fixed while the horizontal one is varied.
The curved boundaries replace the abrupt step in $\vec{M} \cdot \hat{n}$ of the rectangular edges by a gradual variation, spreading the magnetic charges and smoothing the local demagnetizing field, erasing the deep potential wells. Magnons propagate again as extended Bloch waves, restoring the thin-film-like quadratic dispersion.
In this case the unit cell is 890 nm, we have 40 cells, and the central spacing is varied from 10 to 190 nm (N_x, N_y, N_z are kept the same and the cell size is still below l_{ex})[Fig. 3; Appendix B].
Additional simulations with the same geometry but a lattice constant of 610 nm, at which photonic modes arise (relevant for optomagnomechanical designs explored in parallel and future works) [1], show that the lattice constant affects only the periodicity in k, not the shape of the dispersion relation nor the position of the bands. For smaller lattice constants, the Brillouin-zone boundary $k_{\mathrm{BZ}} = \pi/a$ is larger and the period of the dispersion in k is greater, yielding a clearer Brillouin-zone folding.

As the central spacing shrinks, the lower band shifts towards higher frequencies, as expected. Only below a central spacing of 50 nm does the lower flat band disappear yielding a quasi-quadratic dispersion relation, apart from some residual flattening of the bands and a broader linewidth that slightly degrades it.
Another change is observed: for larger spacings the Kittel mode is not clearly distinguishable, masked by the flattening of the bands; as the spacing decreases it becomes visible again and the dispersion approaches that of the thin film.

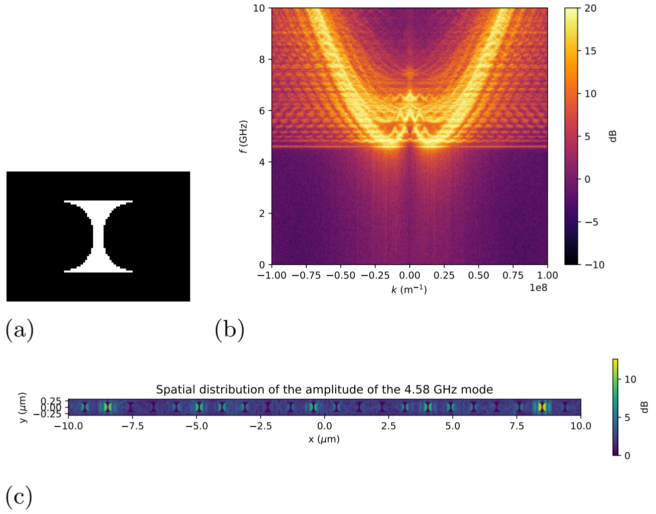

FIG. 3: (a) Unit cell of the concave geometry, with a 50 nm separation hole in a 890 × 630 nm cell. (b) Magnon dispersion relation of the crystal. The lower flat band appears at ∼4.58 GHz. (c) Spatial distribution of the 4.58 GHz mode amplitude, corresponding to the lower flat band.

C. Oval geometry

Finally, we simulate a crystal with an elliptical unit cell. This geometry was selected for two reasons. First, for a moderately elongated ellipse the crystal consists, for the most part, of magnetic material, so we expect a dispersion relation close to that of the thin film. Second, this type of geometry is the one employed in mechanical crystal designs, as it supports well-defined phononic modes; the results could therefore be relevant for future work on magnomechanical interactions.

For elliptical holes that occupy almost the entire unit cell, no lower flat band appears because, as discussed in the concave holes, the smooth edges erase the potential well. Instead, the dispersion shows the quadratic branch with flattened bands superimposed, which degrades it [Fig. 4]. For narrow horizontal semi-axes, the strong transverse confinement of the magnetic material between holes and the sharp edges supports several quantized transverse modes and enhances the demagnetizing field and therefore the potential wells; giving rise to various nearly flat bands [Appendix C].

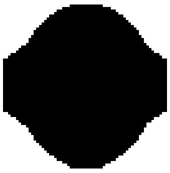

(a)

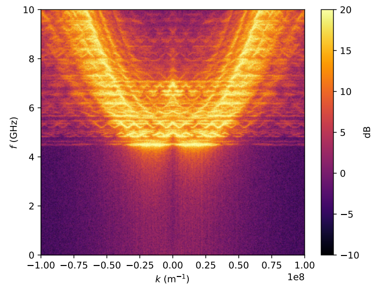

(b)

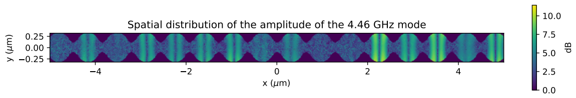

(c)

FIG. 4: (a) Unit cell of the oval geometry, moderate elongated ellipse in a 640 × 640 nm cell. (b) Magnon dispersion relation of the crystal. No lower flat band appears. (c) Spatial distribution of the 4.46 GHz mode amplitude, corresponding to the dispersion minimum.

D. Geometries for condensation

Combining the previous results, the geometries best suited for condensation are those with a clean, gapless dispersion close to that of the thin film, which favours four-magnon thermalization: the moderately elongated elliptical geometry and the concave geometry with 10–50 nm spacing, where no lower flat band is observed.
Using these geometries, we attempted to drive the system towards a Rayleigh–Jeans condensate by parametric pumping, but condensation was not achieved within the explored parameter range. A resonant mode appeared below the dispersion minimum, likely a localized defect state; if its parametric threshold h_{crit} lies below that of the bulk k_{min} mode, it absorbs the pump energy first and saturates early, trapping energy and suppressing the four-magnon scattering that would thermalize the gas into a condensate. A systematic search of the external-field and pumping parameters is left for future work.

V. CONCLUSIONS

We have studied, through micromagnetic simulations, how the spin-wave dispersion relation of a YIG nanostructured waveguide depends on the geometry of a one-dimensional periodic array of holes, with two goals: engineering controllable band structures for magnon condensation, and confining magnons in a cavity.

First, for rectangular holes, the lower flat band shifts towards lower frequencies as the hole width increases, providing a geometric tuning knob. This tunability was exploited to design a magnonic cavity, a promising platform for enhancing magnomechanical coupling, left for future work.

Second, a concave hole geometry was introduced. For central spacings of 50 nm or below, the lower flat band merges with the quadratic branch. Together with the moderately elongated elliptical geometry, which also approaches the thin-film dispersion, are the most suitable candidates for the formation of a magnon Rayleigh–Jeans condensate.

Finally, preliminary attempts to drive the system towards condensation by parametric pumping did not succeed within the explored parameter range, with a resonant mode appearing below the dispersion minimum; completing the search of field and pumping parameters remain as future work.

Acknowledgments

I would like to sincerely thank my advisor, Dr. Marius V. Costache, for his guidance and support throughout this work. I am especially grateful to Pablo Cerrato-Serrano for his constant help, patience, and for teaching me the tools and physics behind this project. Finally, I would like to especially thank my family and friends for their constant support.

[1] D. González Diez, *Rayleigh-Jeans Condensation of quasi-equilibrium magnons in an optomagnomechanical system* (Treball de Fi de Màster), Universitat de Barcelona, 2025.
[2] W.-J. Wu, Y.-P. Wang, J. Li, G. Li, and J.-Q. You, "Microwave-to-optics conversion using magnetostatic modes and a tunable optical cavity," *Laser & Photonics Reviews*, vol. 19, p. 2400648, 2024.
[3] M. Gündoğan, P. M. Ledingham, K. Kutluer, M. Mazzera, and H. de Riedmatten, "Solid state spin-wave quantum memory for time-bin qubits," *Phys. Rev. Lett.*, vol. 114, p. 230501, 2015.
[4] D. Lachance-Quirion, Y. Tabuchi, A. Gloppe, K. Usami, and Y. Nakamura, "Hybrid quantum systems based on magnonics," *Appl. Phys. Express*, vol. 12, p. 070101, 2019.
[5] R. Barbieri et al., "Searching for galactic axions through magnetized media: The QUAX proposal," *Phys. Dark Universe*, vol. 15, pp. 135–141, 2017.
[6] A. Khitun, M. Bao, and K. L. Wang, "Magnonic logic circuits," *J. Phys. D: Appl. Phys.*, vol. 43, p. 264005, 2010.
[7] C. Kittel, "On the theory of ferromagnetic resonance absorption," *Phys. Rev.*, vol. 73, no. 2, pp. 155–161, 1948.

Estudi micromagnètic de l'enginyeria de la relació de dispersió i del confinament de magnons en cristalls magnònics de YIG

Author: Antoni Homar Genovart, ahomarge13@alumnes.ub.edu
Facultat de Física, Universitat de Barcelona, Diagonal 645, 08028 Barcelona, Spain.

Advisor: Marius V. Costache, costache@ub.edu

Resum: Aquest treball investiga cristalls magnònics basats en guies d'ona nanoestructurades de "Yttrium Iron Garnet" (YIG) mitjançant simulacions micromagnètiques realitzades amb mumax3. S'aborden dos objectius principals: dissenyar estructures de bandes d'ones de spin controlables i confinar espacialment magnons en una cavitat. Les estructures consisteixen en una guia d'ona de YIG amb una xarxa periòdica unidimensional de forats de geometria variable. Per a forats rectangulars, apareix una banda plana inferior la freqüència de la qual disminueix en augmentar l'amplada del forat, oferint un mecanisme de control geomètric; aquesta capacitat d'ajust s'aprofita per dissenyar una cavitat magnònica que confina magnons en un defecte mitjançant una transició quadràtica. Les geometries còncava i el·líptica donen lloc a relacions de dispersió quasi sense "band gaps", properes a la de la làmina prima, identificades com les millors candidates per a la condensació de Rayleigh–Jeans de magnons, que les simulacions preliminars de bombeig paramètric encara no han assolit.
Paraules clau: Magnons, Ones de spin, Cristalls magnònics, Condensació de Bose–Einstein, Simulacions micromagnètiques, Física de la matèria condensada.
ODSs: 7 Energia neta i assequible, fita 7.3; 9 Indústria innovació i infraestructures, fita 9.5.

Objectius de Desenvolupament Sostenible (ODSs o SDGs)

1. Fi de les desigualtats		10. Reducció de les desigualtats	
2. Fam zero		11. Ciutats i comunitats sostenibles	
3. Salut i benestar		12. Consum i producció responsables	
4. Educació de qualitat		13. Acció climàtica	
5. Igualtat de gènere		14. Vida submarina	
6. Aigua neta i sanejament		15. Vida terrestre	
7. Energia neta i sostenible	X	16. Pau, justícia i institucions sòlides	
8. Treball digne i creixement econòmic		17. Aliança pels objectius	
9. Indústria, innovació, infraestructures	X		

El contingut d'aquest TFG es relaciona principalment amb l'ODS 9, i en particular amb la fita 9.5, ja que constitueix recerca fonamental orientada a ampliar les capacitats tecnològiques en magnònica, un camp amb aplicacions emergents en computació, transducció i memòries quàntiques. També es vincula amb l'ODS 7, fita 7.3, atès que el control d'ones de spin obre una via cap a paradigmes de computació de baixa dissipació energètica, on la informació es processa sense transport de càrrega i, per tant, sense l'escalfament Joule associat a l'electrònica convencional.

GRAPHICAL ABSTRACT

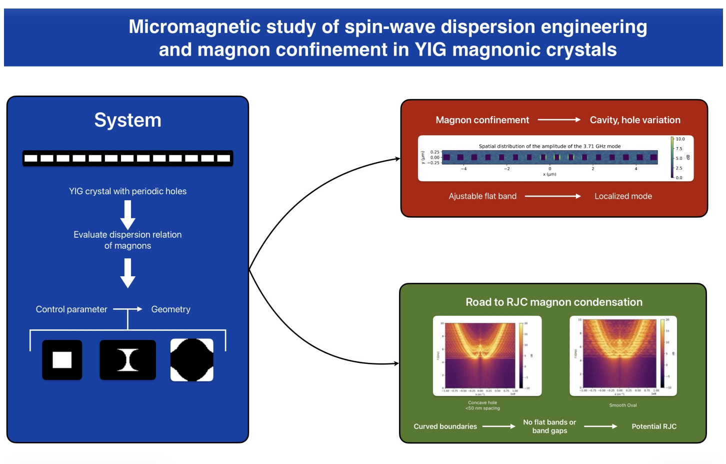

Appendix A: Dispersion relations for the thin film and all rectangular holes

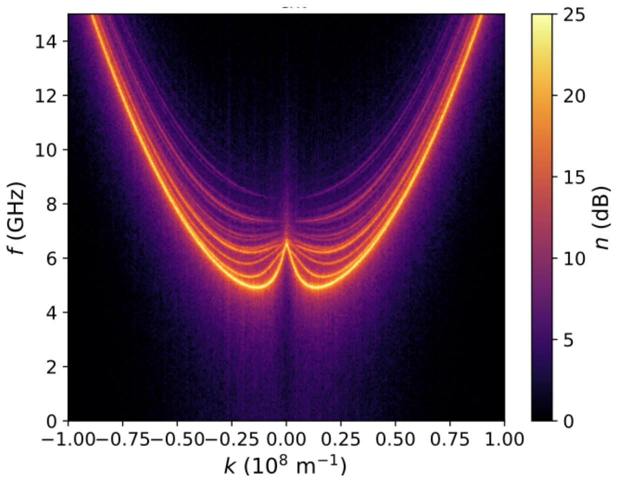

(a)

FIG. 5: Simulated magnon dispersion relation of the thin film.

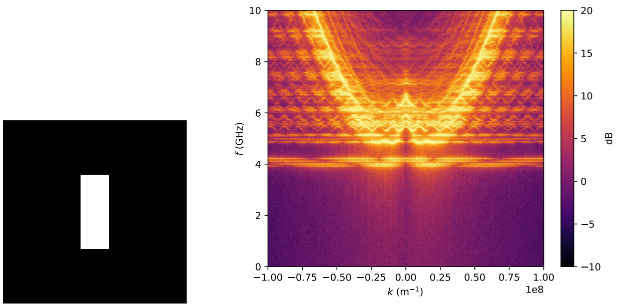

(a) (b)

FIG. 6: (a) Unit cell of the rectangular geometry, with a 100×260 nm hole (black: magnetic material) in a 640×640 nm cell. (b) Simulated magnon dispersion relation of the corresponding crystal.

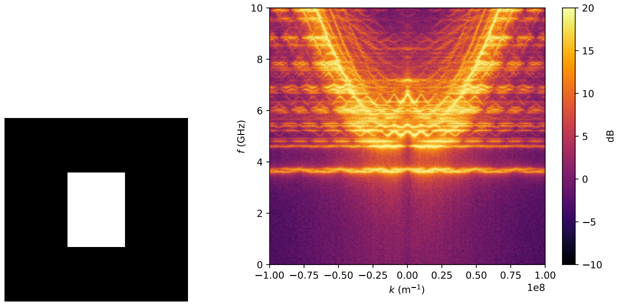

(a) (b)

FIG. 7: (a) Unit cell of the rectangular geometry, with a 200×260 nm hole (black: magnetic material) in a 640×640 nm cell. (b) Simulated magnon dispersion relation of the corresponding crystal.

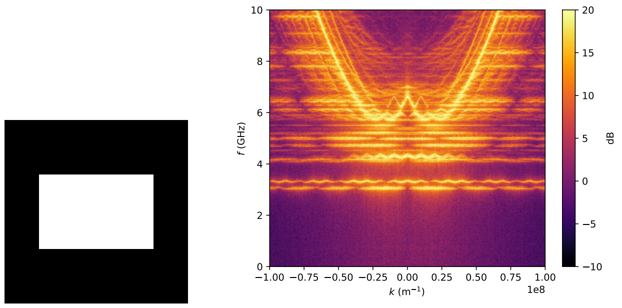

(a) (b)

FIG. 8: (a) Unit cell of the rectangular geometry, with a 400×260 nm hole (black: magnetic material) in a 640×640 nm cell. (b) Simulated magnon dispersion relation of the corresponding crystal.

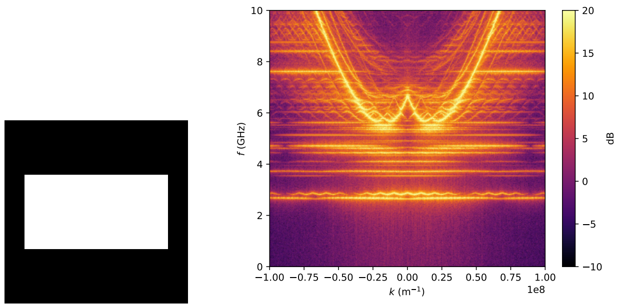

(a) (b)

FIG. 9: (a) Unit cell of the rectangular geometry, with a 500×260 nm hole (black: magnetic material) in a 640×640 nm cell. (b) Simulated magnon dispersion relation of the corresponding crystal.

Appendix B: Dispersion relation for all concave holes

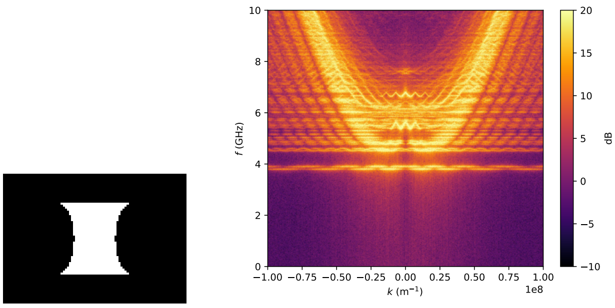

(a) (b)

FIG. 10: (a) Unit cell of the concave geometry, with a 190 nm central spacing(black: magnetic material) in a 890 × 630 nm cell. (b) Simulated magnon dispersion relation of the corresponding crystal.

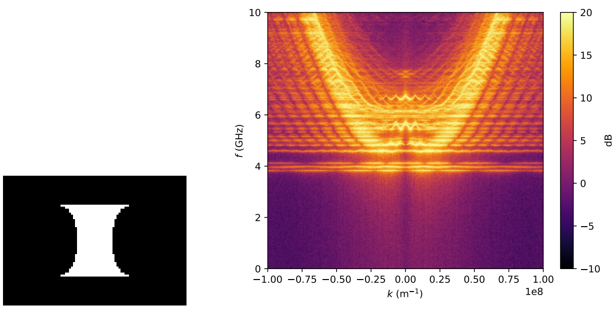

(a) (b)

FIG. 11: (a) Unit cell of the concave geometry, with a 170 nm central spacing(black: magnetic material) in a 890 × 630 nm cell. (b) Simulated magnon dispersion relation of the corresponding crystal.

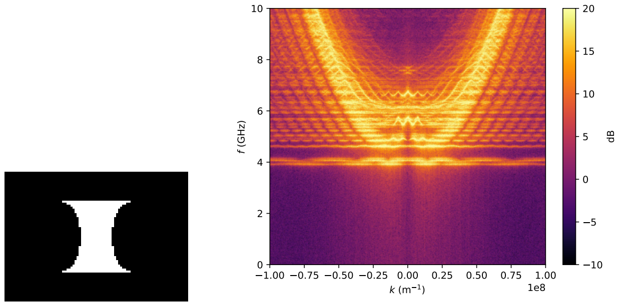

(a) (b)

FIG. 12: (a) Unit cell of the concave geometry, with a 150 nm central spacing(black: magnetic material) in a 890 × 630 nm cell. (b) Simulated magnon dispersion relation of the corresponding crystal.

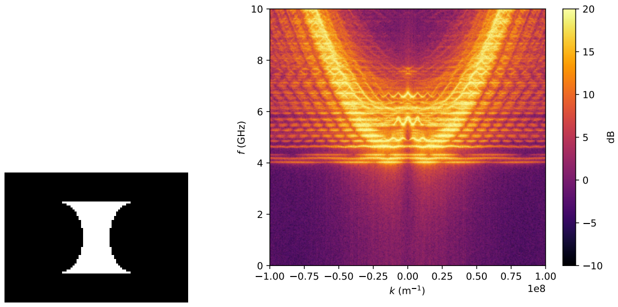

(a) (b)

FIG. 13: (a) Unit cell of the concave geometry, with a 130 nm central spacing(black: magnetic material) in a 890 × 630 nm cell. (b) Simulated magnon dispersion relation of the corresponding crystal.

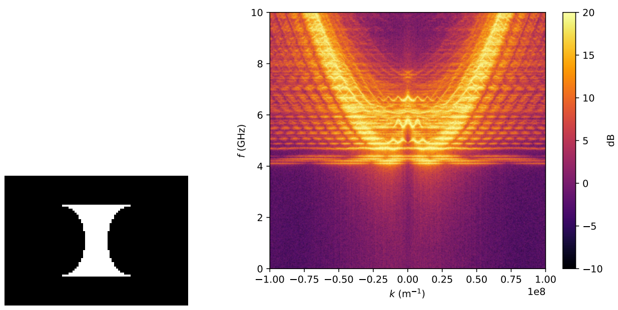

(a) (b)

FIG. 14: (a) Unit cell of the concave geometry, with a 110 nm central spacing(black: magnetic material) in a 890 × 630 nm cell. (b) Simulated magnon dispersion relation of the corresponding crystal.

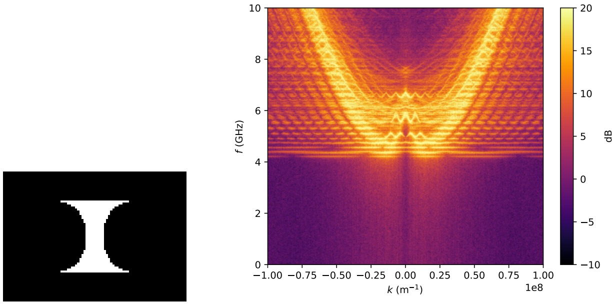

(a) (b)

FIG. 15: (a) Unit cell of the concave geometry, with a 90 nm central spacing(black: magnetic material) in a 890×630 nm cell. (b) Simulated magnon dispersion relation of the corresponding crystal.

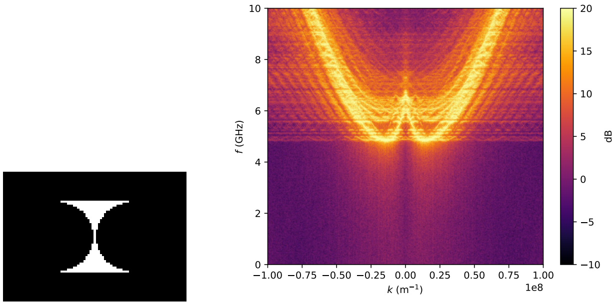

(a) (b)

FIG. 16: (a) Unit cell of the concave geometry, with a 10 nm central spacing(black: magnetic material) in a 890×630 nm cell. (b) Simulated magnon dispersion relation of the corresponding crystal.

Appendix C: Dispersion relation for elliptical geometries

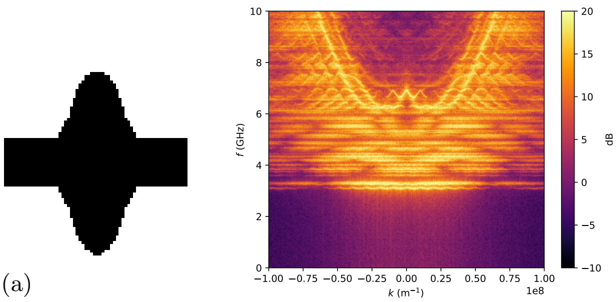

(a)

FIG. 17: (a) Unit cell of the oval geometry, with a (black: magnetic material) in a 640×640 nm cell. (b) Simulated magnon dispersion relation of the corresponding crystal.

Appendix D: Cavity modes

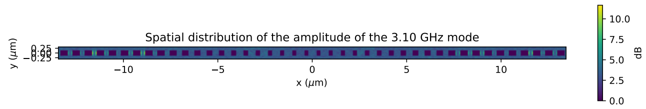

FIG. 18: Real space of the cavity for the 3.10 GHz mode.

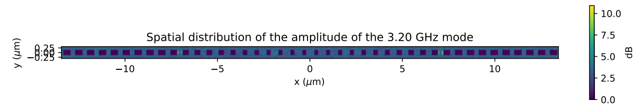

FIG. 19: Real space of the cavity for the 3.20 GHz mode.

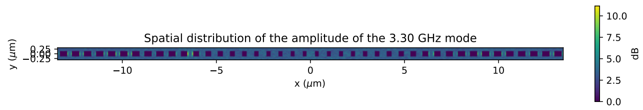

FIG. 20: Real space of the cavity for the 3.30 GHz mode.

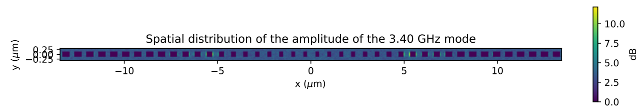

FIG. 21: Real space of the cavity for the 3.40 GHz mode.

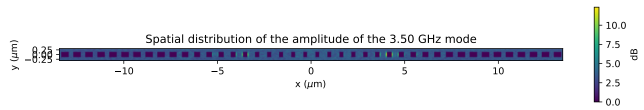

FIG. 22: Real space of the cavity for the 3.50 GHz mode.

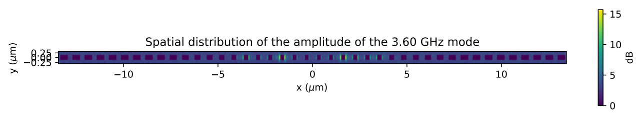

FIG. 23: Real space of the cavity for the 3.60 GHz mode.

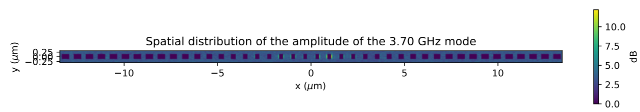

FIG. 24: Real space of the cavity for the 3.70 GHz mode.

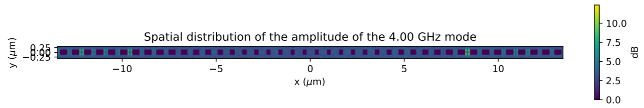

FIG. 25: Real space of the cavity for the 4.00 GHz mode.

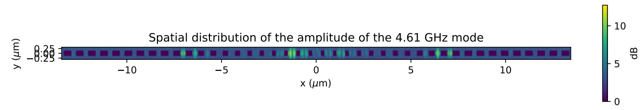

FIG. 26: Real space of the cavity for the 4.61 GHz mode.

Appendix E: Simulation codes

Example simulation in mumax 3.0 for the cavity. All the other simulations have been performed with the same code but adjusting the parameters Nx, Ny, Nx, cx, cy, cz and PBC for each specific case:

```
// --- Grid & cell size (set these numbers to your
    final values) ---
Nx := 4096
Ny := 64
cx := 42*640e-9/Nx
cy := 640e-9/Ny
cz := 400e-9/Nz

setgridsize(Nx, Ny, Nz)
setcellsize(cx, cy, cz)

// --- Periodic boundary conditions ---
setPBC(10, 0, 0)

// --- Geometry mask (PNG) ---
setgeom( imageShape("D:/Apps/mumax3.11/Marius/Toni/
    Cristalls/masc_divergent_r15_c50.png") )
EdgeSmooth = 4

// --- Material parameters (YIG) ---
enabledemag = true
Aex = 3.4e-12
Msat = 0.138e6
Temp = 300
```

```
alpha = 0.0005

// --- Bias field & initial state ---
B_ext = vector(0.15, 0, 0)
m = uniform(1, 0, 0)

// --- Relax to equilibrium ---
relax()
snapshot(m)

// --- Gaussian excitation pulse (spatial mask) ---
mask := newVectorMask(Nx, Ny, 1)
for i:=0; i<Nx; i++{
    for j:=0; j<Ny; j++{
        for k:=0; k<Nz; k++{
            r := index2coord(i, j, k)
            x := r.X()
            y := r.Y()
            z := r.Z()
            By := exp(-pow(x/80e-9, 2))
                * exp(-pow(y/80e-9, 2))
                * exp(-pow(z/80e-9, 2))
            mask.setVector(i, j, k, vector(0, By, 0))
        }
    }
}

A := 0.01
TableAdd(B_ext)

// temporal gaussian pulse
B_ext.add(mask, A*exp(-pow((t-5e-10)/2e-11, 2)))

// --- Time settings & output ---
fmax := 40e9
pasT := 1/(2*fmax)

MaxDt = pasT/2
tableautosave(pasT)

// Save magnetization
autosave(m.comp(1), pasT)

run(8*1024*pasT)

snapshot(m)
```